Proceedings of the Research Institute of Atmospherics,
Nagoya University, vol. 18 (1971)

IMPROVED RADIO MAPPING OF THE SUN

Masakazu ARISAWA

Abstract

Improved data processing has been applied to the T-shaped 3-cm radioheliograph at Toyokawa. Unwanted harmonics of the signal corresponding to the frequency range beyond the cut-off spatial frequency have been removed. Phase error between the phase centers of the N−S and E−W arrays, which is peculiar to the T-shaped radioheliograph, has also been removed. Smoothing in two dimensions has been made to eliminate the effect of side lobes. It is shown by figures how an original map is refined, step by step, by computer processing, which is a good example of antenna-computer coupling to complete the whole system.

1. Introduction

Two radioheliographs have long been in operation; one at Fleurs, Australia on 21 cm with HPBW of 2!2 (Christiansen et al. 1957) and the other at Stanford, U. S. A. on 9 cm with HPBW of 3!1 (Bracewell and Swarup 1961). Daily maps obtained by these heliographs are published regularly in the 'Solar Geophysical Data' issued by ESSA, U. S. A.. In both cases, scanning of the sun is made like a television, the east-west scan by the drift of the sun and the north-south by shifting the beam to a correct position successively each time when the east-west scan is finished.

For a Fleurs map, a frame is composed of 13 lines with a uniform spacing of 2.67 arc minutes confined between the north and south limbs of the sun, and each line is sampled 15 times at the same intervals of 2.67 arc minutes. The number of picture elements, then, is 195, which is less than minimum necessary number of samples. The observed values are printed in digits and contours are sketched by hand.

For a Stanford map, a frame is composed of 21 lines with a uniform spacing of

about 1.81 arc minutes and each line is sampled 25 times at intervals of about 1.63 arc minutes. Thus 525 picture points exist in a frame, 38 arc minutes in the north-south side and 41 arc minutes in the east-west side. The sampling intervals are sufficiently short with a margin of more than 50 percent. The observed values are printed for display and contours are drawn by machine. This is done after partially smoothing the picture by taking running means of each nine points, but the effect of negative beam is still left.

As for the 3-cm radioheliograph at Toyokawa, the antenna system is described in detail by Tanaka et al. (1970) in the last volume. It is considerably different from those described above. Firstly, antenna arrays are T-shaped instead of cross-shaped which is more sensitive to phase error. Secondly, the beam-width is as sharp as 1!5 in HPBW. Lastly, sensitivity to radio emissions from the active region on the sun is lower due to its spectrum and also due to the limitation in the size of element antennas. A difficulty arising from the second speciality has been overcome by the 'skip scanning' program, which is described in the last volume. At that time, however, data processing was in an early stage, and the first and last specialities mentioned above were left untouched. Recently, considerable progress has been made in obtaining an improved map by processing 4095 picture elements, which are four times the minimum necessary number of samples. This redundancy is connected with insufficient sensitivity of the receiver system. The first basic improvement is the reduction of noise which is described in Section 3. Another improvement is described in Section 4, where it is shown how the phase problem peculiar to T-shaped antenna has been solved. In Section 5, it is shown by a series of figures how the original map is refined step by step by the above mentioned processing. It clearly shows that the antenna system cannot be completed without the aid of computer processing.

2. Basic Equations for the T-Shaped Antenna

For the discussion in the following sections, let us recall first the well-known theory relevant to the T-shaped antenna (Swarup, 1961). It is known that the field pattern of a highly directional antenna is related to the Fourier transform of aperture distribution. Let $g(x, y)$ and $h(x, y)$ be the aperture distribution over the two antennas of the phase-switched interferometer, where x and y are rectangular coordinates and the origin is taken at an arbitrary point in the aperture, the corresponding field patterns $G(l, m)$ and $H(l, m)$ are given by the following equations:

$$G(l, m) = \text{const.} \int\int_{-\infty}^{+\infty} g(x, y) \exp[-j2\pi(lx+my)/\lambda]\, dxdy \quad \cdots\cdots\cdots \quad (1)$$

$$\tilde{H}(l, m) = \text{const.} \int\int_{-\infty}^{+\infty} h(x, y) \exp[-j2\pi(lx+my)/\lambda]\, dxdy \quad \cdots\cdots (2)$$

where l and m are direction cosines corresponding to x and y, respectively. In a T-shaped antenna the phase centers of the two arms are not coincident, and if we choose the origin to be at the center of the long arm, Eqs. (1) and (2) reduce to

$$G(l, m) = \text{const.} \sin(32\pi dl/\lambda) / \sin(\pi dl/\lambda) \quad \cdots\cdots (3)$$

$$= \text{const.} \sum_{r=1}^{16} 2\cos[(2r-1)\pi dl/\lambda] \quad \cdots\cdots (4)$$

$$H(l, m) = \text{const.} (\sin(16\pi dm/\lambda) / \sin(\pi dm/\lambda)) \exp[j(16\pi dm/\lambda)] \cdots\cdots (5)$$

In a phase-switched interferometer the two antennas are alternately connected in phase and out of phase, and the difference component is recorded. The power at the input of the receiver is given by $(G+H)(G+H)^*/2$ and $(G-H)(G-H)^*/2$ for the in-phase and out-of-phase condition respectively. The reception pattern is

$$P_m = [(G+H)(G+H)^* - (G-H)(G-H)^*]/2 = 2\mathrm{Re}(GH^*) \quad \cdots (6)$$

and therefore, substituting Eqs. (3) and (5) into Eq. (6), we get

$$P_{tee} = \text{const.} [\sin(32\pi dl/\lambda) / \sin(\pi dl/\lambda)] [\sin(32\pi dm/\lambda) / \sin(\pi dm/\lambda)] \quad \cdots (7)$$

for the reception pattern of the T-shaped antenna.

It is seen that the power reception pattern of a T-shaped antenna is exactly the same as that of the cross.

If $T_b(l, m)$ denotes the brightness distribution, the output of the antenna can be written as

$$T_a(l, m) = \int\int_{-\infty}^{+\infty} T_b(l', m') \tilde{P}_{tee}(l-l', m-m')\, dl'\, dm' \quad \cdots\cdots (8)$$

$$= \int_{-\infty}^{+\infty} \tilde{H}'(m-m')\, dm' \int_{-\infty}^{+\infty} T_b(l', m') \tilde{G}(l-l')\, dl' \quad \cdots\cdots (9)$$

where

$$H' = \text{const.} \sin(32\pi dm/\lambda) / \sin(\pi dm/\lambda) \quad \cdots\cdots (10)$$

$$= \text{const.} \sum_{r=1}^{16} 2\cos[(2r-1)\pi dm/\lambda] \quad \cdots\cdots (11)$$

and $\sim$ denotes mirror image.

As $G(l'-l)$ is the field pattern of a highly directional antenna, we can write

$$\int_{-\infty}^{+\infty} T_b(l', m')\,\tilde{G}(l-l')\,dl' \simeq \text{const. } T_b(l, m') \quad \cdots\cdots (12)$$

and therefore, Eq. (9) reduces to

$$T_a(l=\text{const.}, m) = \int_{-\infty}^{+\infty} T_b(l=\text{const.}, m')\,\tilde{H}'(m-m')\,dm' \quad \cdots\cdots (13)$$

Similarly we get

$$T_a(l, m=\text{const.}) = \int_{-\infty}^{+\infty} T_b(l', m=\text{const.})\,\tilde{G}(l-l')\,dl' \quad \cdots\cdots (14)$$

We can replace Eq. (8), a two dimensional convolution, by Eqs. (13) and (14), one dimensional convolutions.

Let us consider Eqs. (13) and (14) in the spatial frequency region. Then

$$T_a(l=\text{const.}, s_y) = T_b(l=\text{const.}, s_y)\,\tilde{H}'(s_y) \quad \cdots\cdots (15)$$

and

$$T_a(s_x, m=\text{const.}) = T_b(s_x, m=\text{const.})\,G(s_x) \quad \cdots\cdots (16)$$

where s_x and s_y express the spatial frequency of the x and y components, respectively. It follows from Eqs. (4) and (11) that $T_a(l=\text{const.}, s_y)$ and $T_a(s_x, m=\text{const.})$ have only odd harmonics and there is a cut-off for all harmonics greater than $31d/2\lambda$.

3. Reduction of Noise

It is clear from the above theory that if there are spatial harmonics beyond the cut-off frequency in the observed record, they certainly originate in the receiver or in some outside disturbances. These unwanted harmonics cannot be filtered out by using a simple electric circuit, but they can be easily removed with a computer by simply eliminating the signal beyond the cut-off frequency in the frequency domain.

This process would be unnecessary when the signal from the sky is strong enough

compared with the system noise, so that a theoretically minimum sampling frequency for spatial cut-off would be sufficient for further processing. In the presence of considerable noise, however, a low-pass filter should be applied first in such a way as not to distort the signal within the spatial cut-off frequency. Then, the filtered signal should be sampled at a frequency sufficiently high to reproduce its waveform. It is on such a condition that the above method of reducing noise can be applied. In practice, there is a limit to the sampling frequency and data handling capacity, but a sampling frequency twice that of the theoretically minimum value for negligible system noise is considered to be minimum. The system of the Toyokawa radioheliograph is so designed as to facilitate data processing, and the sampling frequency is always just twice independent of the declination of the sun, so that unwanted noise beyond the cut-off frequency can be easily rejected.

4. Correction of the Phase Error

Errors in phase adjustment of the antenna decrease directivity and increase side lobe levels. The phase adjustment is highly critical in a T-shaped antenna, since any spatial Fourier component is measured by a single pair of array components. An error which seriously affects the reception pattern of asymmetrical phase-switched systems, like a T-shaped antenna, is a phase error between the phase centers of north-south and east-west arrays. Let us call it a fixed phase error δ_0. This error sometimes occurs because of the change of length of the transmission lines connecting the two arrays. It is mainly due to temperature variations.

In the presence of a fixed phase error δ_0, Eq. (5) is replaced by

$$H(l, m) = \text{const.}\ [\sin(16\pi dm/\lambda) / \sin(\pi dm/\lambda)]\ \exp[j(16\pi dm/\lambda+\delta_0)] \quad \cdots (17)$$

and, therefore, from Eq. (6) the reception pattern of the T-shaped antenna is given by

$$P = \text{const.}\ [\sin(32\pi dl/\lambda) / \sin(\pi dl/\lambda)]\ [(\sin(32\pi dm/\lambda) / \sin(\pi dm/\lambda))\cos\delta_0 - 2(\sin^2(16\pi dm/\lambda) / \sin(\pi dm/\lambda))\sin\delta_0] \quad \cdots (18)$$

where

$$2\sin^2(16\pi dm/\lambda) / \sin(\pi dm/\lambda) = \sum_{r=1}^{16} 2\sin[(2r-1)\pi dm/\lambda]. \quad \cdots (19)$$

In the presence of a fixed phase error, the field pattern of the T-shaped antenna in the N-S direction consists of two components, even and odd functions.

It follows from Eq. (15) that

$$T_a(l=\text{const.}, s_y) = T_b(l=\text{const.}, s_y)\tilde{H}''(s_y), \quad \cdots\cdots (20)$$

or separating the sine and the cosine terms, we obtain

$$T_{ac}(s_y) + jT_{as}(s_y) = (T_{bc}(s_y) + jT_{bs}(s_y))(H_c(s_y)\cos\delta_0 + jH_s(s_y)\sin\delta_0). \quad \cdots\cdots (21)$$

If $H_c(s_y)$ and $H_s(s_y)$ are normalized using Eqs. (11) and (19), Eq. (21) reduces to

$$T_{ac}(s_y) + jT_{as}(s_y) = (T_{bc}(s_y) + jT_{bs}(s_y))(\cos\delta_0 + j\sin\delta_0), \quad \cdots\cdots (22)$$

or separating the real and the imaginary part, we obtain

$$T_{bc}(s_y) = T_{ac}(s_y)\cos\delta_0 + T_{as}(s_y)\sin\delta_0 \quad \cdots\cdots (23)$$

and

$$T_{bs}(s_y) = T_{as}(s_y)\cos\delta_0 - T_{ac}(s_y)\sin\delta_0. \quad \cdots\cdots (24)$$

If we perform the Fourier transform of the data in the N-S direction, we can know $T_{ac}(s_y)$ and $T_{as}(s_y)$. Therefore, knowing δ_0, we can get $T_{bc}(s_y)$ and $T_{bs}(s_y)$ from Eqs. (23) and (24). By performing the inverse Fourier transform of $T_b(s_y)$ we can get a corrected brightness distribution $T_b(l_0, m)$ for a certain direction l_0. By performing this process 63 times we can draw a contour map of brightness corresponding to the observation with no fixed phase error. At present δ_0 is determined by trial and error as shown in Section 5.

It should be mentioned here that it is possible to determine δ_0 by making an additional observation using the N-S arm of the T-shaped antenna as the adding interferometer. The power pattern of the adding interferometer can be expressed as follows;

$$P_a = [\sin(16\pi dm/\lambda)/\sin(\pi dm/\lambda)]^2 = 16 + \sum_{r=1}^{15} 2(16-r)\cos(2r\pi dm/\lambda) \quad \cdots (25)$$

$$T_a^+(s_y) = \tilde{P}_a(s_y)T_b(s_y) = T_{ac}^+(s_y) + jT_{as}^+(s_y) \quad \cdots\cdots (26)$$

In the case of the T-shaped antenna, on the other hand, the Fourier transform of the sum of the data in the E-W direction is derived from Eq. (15) as follows;

$$\sum_{i=1}^{63} T_a(l_i, s_y) = \tilde{H}(s_y) \sum_{i=1}^{63} T_b(l_i, s_y). \quad \cdots\cdots (27)$$

If we put

$$S T_a(s_y) = \sum_{i=1}^{63} T_a(l_i, s_y) = S T_{ac}(s_y) + j S T_{as}(s_y) \quad \cdots\cdots (28)$$

and

$$S T_b(s_y) = \sum_{i=1}^{63} T_b(l_i, s_y) = S T_{bc}(s_y) + j S T_{bs}(s_y), \quad \cdots\cdots (29)$$

we get the same equation as Eqs. (23) and (24) as follows;

$$S T_{bc}(s_y) = S T_{ac}(s_y) \cos \delta_0 + S T_{as}(s_y) \sin \delta_0 \quad \cdots\cdots (30)$$

and

$$S T_{bs}(s_y) = S T_{as}(s_y) \cos \delta_0 - S T_{ac}(s_y) \sin \delta_0. \quad \cdots\cdots (31)$$

As we can trust the information on the phase of $T_a(s_y)$, it follows that

$$T^+_{as}(s_y) / T^+_{ac}(s_y) = S T_{bs}(s_y) / S T_{bc}(s_y) \quad \cdots\cdots (32)$$

and therefore, substituting Eqs. (30) and (31) into Ep. (32) we get

$$\delta_0 = \tan^{-1}[\{T^+_{ac}(s_y)\, S T_{as}(s_y) - T^+_{as}(s_y) S T_{ac}(s_y)\} / \{T^+_{as}(s_y) S T_{as}(s_y) + T^+_{ac}(s_y)\, S T_{ac}(s_y)\}]. \quad \cdots\cdots (33)$$

We can know δ_0 more exactly if we find the average of δ_0 near the fundamental spatial frequency. It is to be remarked that though $T^+_a(s_y)$ does not contain odd harmonics, we can calculate them from the sampling theorem for the frequency domain.

5. Actual Procedure of Data Processing at Toyokawa

As has been described in the last volume, scanning is performed in a complicated order with positive and negative beams, alternately. The sky level to be subtracted from all the data is determined first by taking the mean of observed values during one scan which is remotest from the sun. Then the samples are rearranged in a correct order in such a way as if the scanning were uniform instead of 'skip scanning'. At the same time, the sign of samples corresponding to negative beams is inverted,

and the values are normalized by a flux value obtained from total flux observations. Thus we can get the original map as shown in Fig. 1 using a contour program.

Fig. 2 shows the effect of smoothing in two dimensions as described in the last volume, which can be performed easily owing to the well-fitted sampling interval. Fig. 3 is another version of Fig. 1 where the method of reducing noise mentioned in Section 3 is applied. Fig. 4 shows the result of applying both smoothing and noise rejection.

The correction of the phase error between the phase centers described in Section 4 is performed by looking at the reproduced original scan curves around the highest peak as shown in Fig. 5(a) and find a value of δ_0 by experience. After a few trial, the waveforms becomes acceptable as shown in Fig. 5(b), and thus the value of δ_0 is determined.

In this way, we can get two final maps. One is the map after phase correction and noise reduction as shown in Fig. 6, and the other is the most refined map as shown in Fig. 7 where the data processing described here is fully applied.

Acknowledgements

The author wish to express his sincere thanks to Prof. H. Tanaka, Messrs. S. Énomé and M. Ishiguro of Toyokawa Observatory for their valuable discussions. He thanks also Mr. T. Takayanagi and Miss K. Nakanishi for their assistance in data reductions. He is grateful to the division of Solar Physics of Tokyo Astronomical Observatory for the sunspot drawing.

References

Bracwell, R. N., and Swarup, G.: The Stanford Microwave Spectroheliograph Antenna, a Microsteradian Pencil Beam Interferometer, IRE Trans. Ant. and Prop., **AP-9**, 1, 22 (1961).

Christiansen, W. N., Mathewson, D. S., and Pawsey, J. L.: Radio Pictures of the Sun, Nature, **180**, 9, 944 (1957).

Swraup, G.: Studies of Solar Microwave Emission using a Highly Directional Antenna, scientific report, **13**, Stanford Electronics Lab. (1961).

Tanaka, H., Énomé, S., Torii, C., Tsukiji, Y., Kobayashi, S., Ishiguro, M., and Arisawa, M.: 3-cm Radioheliograph, Proc. Res. Inst. Atmospherics, Nagoya Univ., **17**, 57 (1970).

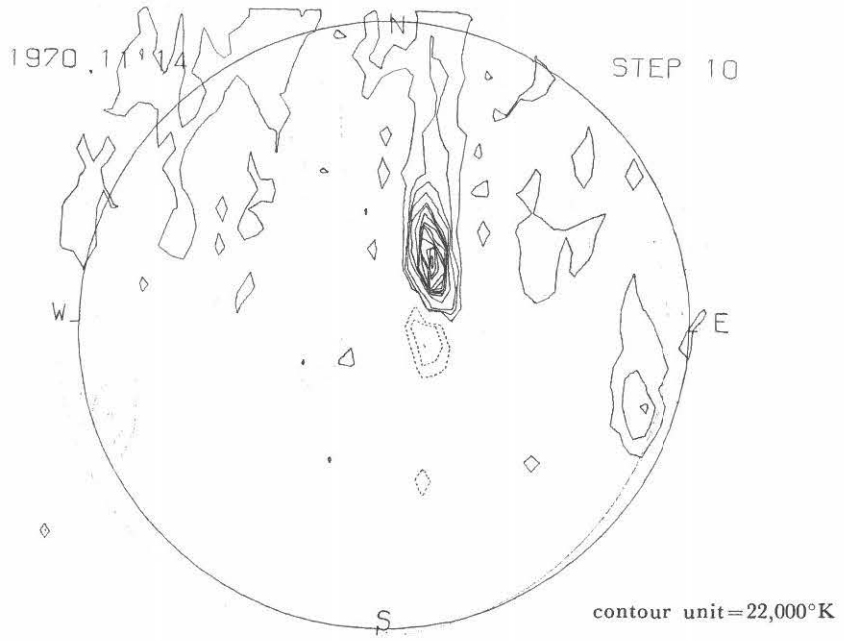

Fig. 1. The original map of brightness.

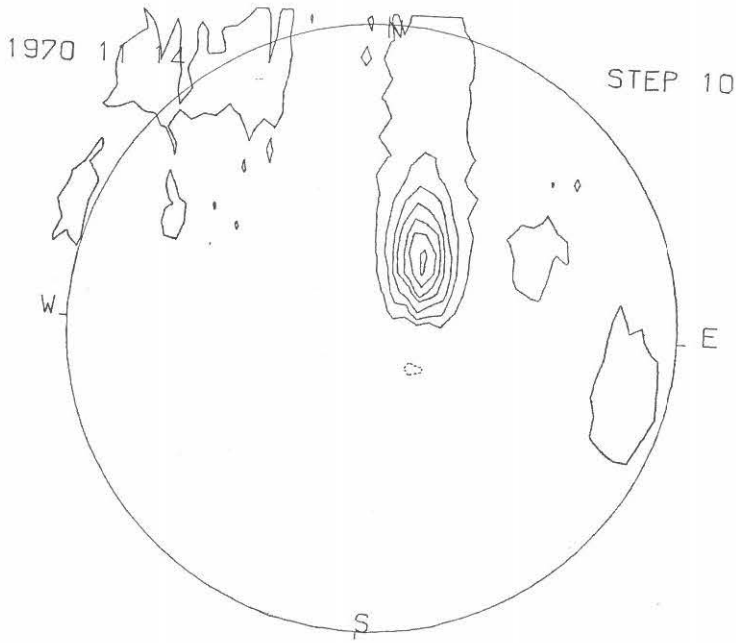

Fig. 2. The contour map after smoothing.

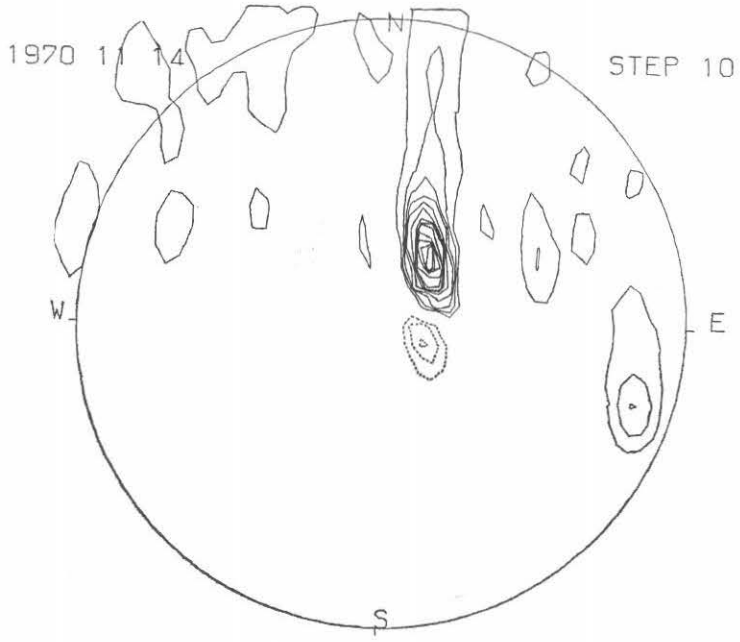

Fig. 3. The contour map after noise reduction.

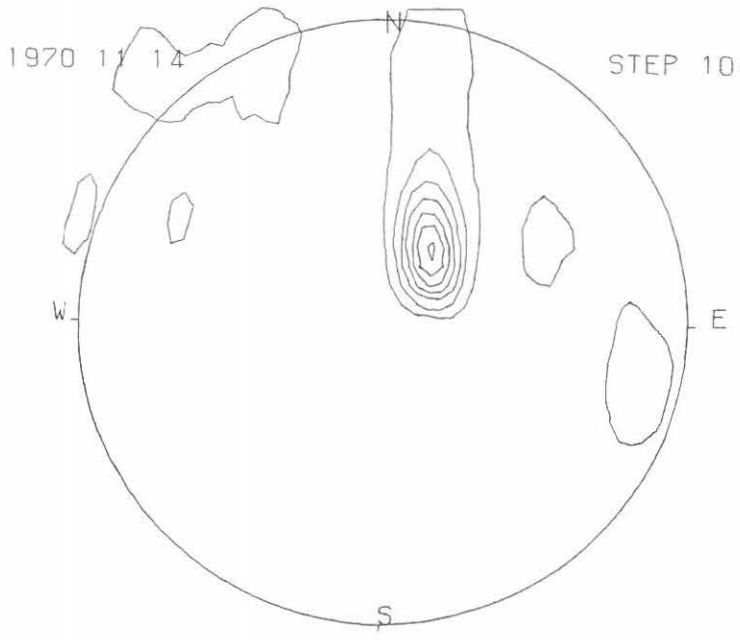

Fig. 4. The contour map after smoothing and noise reduction.

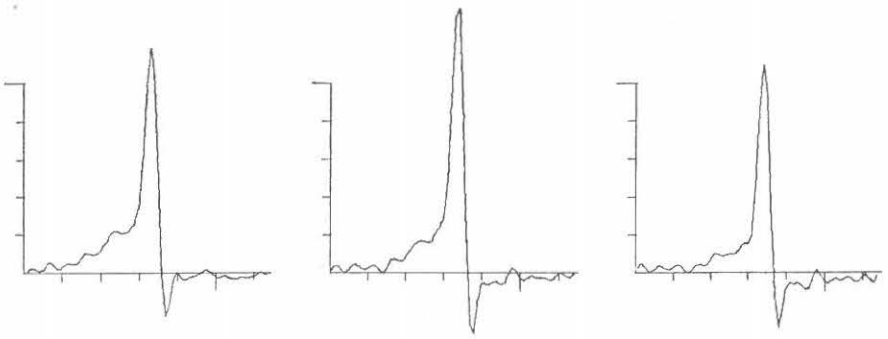

Fig. 5(a). The original scan curves in the N-S direciton around the highest peak.

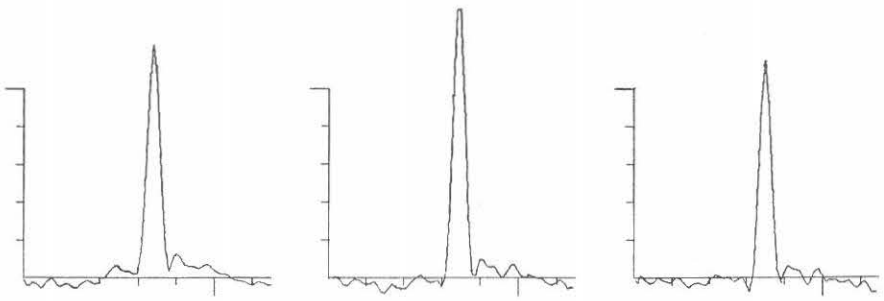

Fig. 5(b). The curves after phase correction.

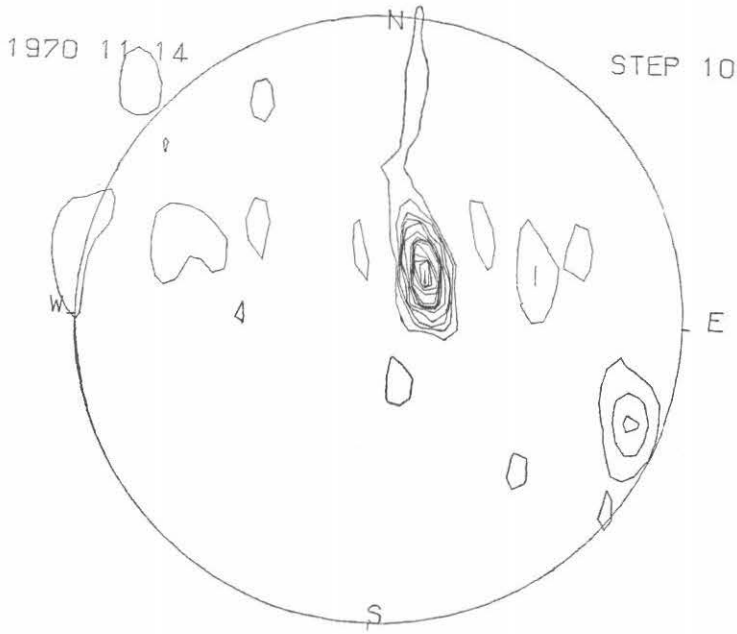

Fig. 6. The contour map after phase correction and noise reduction.

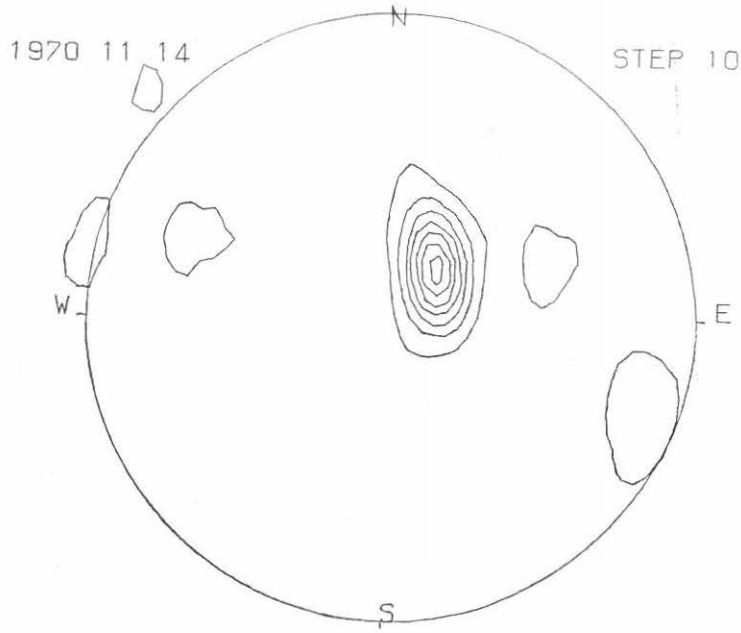

Fig. 7. The most refined map after phase correction, noise reduction and smoothing.

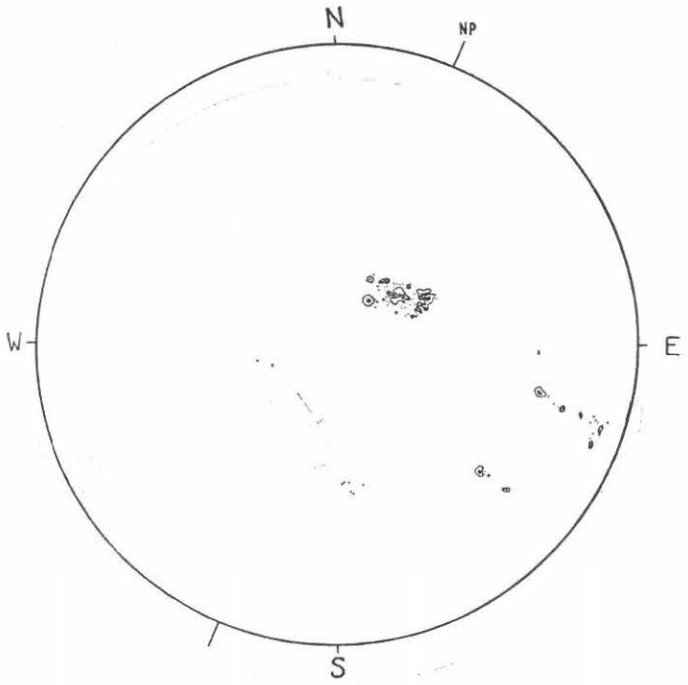

Fig. 8. Sunspot drawing on the same day (Tokyo astronomical observatory).

Errata for the paper in Vol. 17 "3-cm Radioheliograph" by Tanaka et al.

Page	Row	for	read
61	Eq. (6)	$\{I-(1/J)$	$\{I-(1/J)\}$
62	Eq. (14)	$\sin \varphi_m - f_{s0}/K$	$\sin \varphi_m - f_{s0}\varphi_m/K$
62	Eq. (15)	$\varphi_m/12$	$\varphi_m^2/12$
63	Eq. (14)	(14)	(14)′
63	Eq. (15)	(15)	(15)′
65	Eq. (17)	$s\cdot\sin\omega - f_s(t-t_0)$	$s\cdot\sin\omega + f_s(t-t_0)$
65	Eq. (20)	$\cos\gamma\cos\delta\cos kT$	$\cos\gamma\cos\delta\cos kT_1$
69	8	date	data
69	11	explain	express
64	Fig. 3	put $\leftarrow \Delta N \rightarrow$ between centers of circles	